Disclaimer: this is a non peer-reviewed publication.

More specifically, this manuscript has undergone peer-review for Nature Climate Change. It was not accepted, for not being novel / significant enough.
As of 24th October 2020, we have no intention of submitting it elsewhere.

Global decline of deep water formation with increasing atmospheric CO_2

Céline Heuzé[1*], Martin Mohrmann[2], Ellen Andersson[2] and Emelie Crafoord[1]
[*]corresponding author: celine.heuze@gu.se
[1] Department of Earth Sciences, University of Gothenburg, Gothenburg, Sweden
[2] Department of Marine Sciences, University of Gothenburg, Gothenburg, Sweden

Abstract

Deep water formation is not only the driver of the global ocean circulation; by sending heat and carbon to the deep ocean, it is also crucial for climate change mitigation. Yet its future is uncertain: will it slow down as stratification increases, emerge in polar regions as the wind starts blowing over previously ice-covered waters, or intensify with increased evaporation? Here we present the first global study of the evolution of deep water formation as atmospheric CO_2 concentration increases, using the latest generation of Earth System models (CMIP6). We show that open ocean deep convection stops globally shortly before 600 ppm, mostly in response to increased stratification, but that deep water formation continues under a different regime. Deep convection does not emerge in ice-freed regions. The mechanism is self-reinforcing, as less mixing also increases stratification and modifies heat fluxes, with most oceanic regions gaining even more heat.

Main text

By establishing a direct connection between the sea surface and the ocean, deep water formation is crucial for ventilation and a driver of the global ocean circulation[1,2,3]. Moreover, by bringing excess anthropogenic heat and carbon to the deep ocean where they can be stored instead of staying in the atmosphere, deep water formation in fact currently mitigates climate change[4,5]. There are many regions where "chimneys" of deep water formation have been observed. The first such region to be monitored was in the Western Mediterranean, where strong winds blowing from the south of France in winter cause very deep mixed layers[6]. It has since been found to also occur in the Eastern Mediterranean, in the Adriatic and Aegean seas[7]. The most "famous" regions are in the North Atlantic, namely in the Labrador – Irminger seas and in the Nordic Seas[8,9,10,11,12]. There, deep waters regularly form as a result of the strong winds blowing from Greenland[8,9] and sea ice processes[8,9,13]. These same two processes cause deep mixing in the enclosed East Sea / Sea of Japan[14]. The last known location in the northern hemisphere is by Rockall Trough (north of Scotland), again in response to strong winds[15]. At the other end of the world in the Southern Ocean, current observations suggest that deep waters are formed mostly from shelf processes[16], so that deep convection happens more seldom, in association with open ocean polynyas[8,9,17,18].

The future of deep water formation is far from obvious. In the strongly stratified Arctic Ocean, deep water formation has hardly ever been observed[12]; yet, some modelling results[19] project that deep convection will become commonplace there, as sea ice decline means that the wind can start mixing this ocean. Observation-based results disagree and show in fact an increase in stratification and a decrease in mixed layer depth[20]. In the Nordic Seas, observations suggest that the necessary surface salinization may still be accomplished by enhanced evaporation if brine rejection decreases[21], and deep water formation could hence continue unhindered. And in the Southern Ocean, open ocean deep convection is either expected to cease in response to surface freshening[22], or to restart as part of an ongoing poorly-observed low-frequency cycle[23], of which the re-opening of the Weddell Polynya in the last years[24] would be a sign.

It does not help that so far, such studies have investigated individual regions in isolation, without considering the rest of the world. Yet, deep water formation rates in the North Atlantic and Southern Ocean are linked[25], and we know that signals can spread within years through deep waters globally[26,27]. This study was therefore initiated to answer this question: is deep water formation stopping globally, or are the volumes formed conserved while only the locations change? Here we present the first global assessment of the future of deep water formation in response to ongoing and projected increased atmospheric CO_2 concentrations. We are about to show that deep water formation declines dramatically quickly and globally, and changes regime shortly before 600 ppm.

Open ocean deep convection stops, globally

To explore the sensitivity of global deep water formation to sea ice, wind and stratification under anthropogenic climate change (increased CO_2), we examined 30 models that have submitted their ocean, atmosphere and sea ice output to the Coupled Model Intercomparison Project phase 6 (CMIP6[28], models listed in supplementary Table 1). We use the "one percent CO_2" experiment as a proxy for short-term climate change, as this experiment represents the range of atmospheric CO_2 increase that is expected throughout the 21st century[29] and contains output from a wide variety of models. Our approach is unique in that we present the evolution of the mixed layer depth or "MLD" as a function of atmospheric CO_2 levels instead of time, to determine its sensitivity.

The models produce deep waters at the locations that are known as sites of deep convection in the real ocean[8,9] (Figs 1 and 2). In the North Atlantic, all models have deep mixing in the subpolar gyre, in the so-called Nordic or GIN (Greenland, Iceland and Norwegian) seas, and by Rockall. Only one model forms deep water in the Arctic already at low CO_2 concentrations. As atmospheric CO_2 levels approach 600 ppm, i.e. by 2060[29], most models stop having mixed layers that exceed 1000 m, i.e. stop deep convection, and instead stabilise around 500 m depth (thick black line in inserts, Fig. 1). Mixed layers deepen on average in the Arctic, but only the 10% most extreme models initiate occasional deep convection there (pale shading in inserts). In the Mediterranean Sea, deep water formation in the models is rare; for the majority of models, MLD in the western site falls below 1000 m around current CO_2 levels; the eastern site continues with occasional deep convection but exhibits a decrease in its strongest models. Finally, as already pointed out by ref [30], the modelled Southern Ocean exhibits open ocean deep convection over too large an area, too often, and too deep, especially in the Weddell Sea. Yet we find the same trend as in the rest of the world: no open ocean deep convection after 600 ppm, and a stabilisation of mixed layers around 500 m depth.

Cessation of open ocean deep convection does not mean cessation of deep water formation (supplementary Fig. 1). The volume of deep water formed as indicated by the Meridional Overturning Circulations decreases sharply until 600 ppm, as mixed layers fall below 1000 m depth, and then decrease more gently to about half their original value on average. The key result of this study is then that, globally, deep water formation switches from high volumes produced by open ocean deep convection (admittedly too often in the model version of some regions) to halved volumes, likely spanning from mixed layers hardly 500 m deep, and that this switch occurs at atmospheric CO_2 levels that we are expected to reach in the coming twenty to forty years. But why is deep convection stopping so soon?

Sea ice is gone; stratification increases globally; winds hardly change

We just saw that deep water formation decreases sharply as atmospheric CO_2 concentration increases, globally. In the literature, deep water formation and more generally vertical mixing are the result of the interplay of up to three processes: stratification, wind, and sea ice formation[8,9]. As found in other CMIP6 runs, the Arctic[31] and Antarctic[32] sea ice disappears as atmospheric CO_2 increases. By the end of the one percent CO_2 run, the vast majority of models are ice-free at both poles even in winter (supplementary Fig. 2 and corresponding trends in total sea ice volume on Fig. 3).

In an ice-free, CO_2-rich world, stratification increases. The multi-model mean trend in stratification (see Methods) is a clear, global increase, with some models increasing their stratification by up to 2 kg m^{-3} on average around 80°N (Fig. 3). For reference, 2 kg m^{-3} is a typical model difference in potential density between the surface and 4000 m depth averaged over 80°N at the beginning of the run (not shown). The cause of this increase in stratification depends on the location: freshening over the Arctic; combined freshening and warming in the subpolar North Atlantic and Nordic Seas; and warming stronger than the opposing trend in salinification at lower latitudes (supplementary Fig. 3). Over the Southern Ocean, the patterns are similar although even more zonal: freshening only closest to the continent, then freshening and warming at high latitudes, and finally warming opposed by a salinification north of 40°S (Polar Front, Fig. 3 and supplementary Fig. 4). The trends in salinity are consistent with local sea ice volume decrease (i.e. reduced brine rejection) and the ongoing destruction of the global ice sheets[33], as well as increased evaporation at low latitudes[33]. Rather obviously, temperature at the top of the ocean increases as CO_2 levels increase.

Changes in surface wind in a warming world are debated. Over land, a stilling had been detected and attributed in parts to changing atmospheric circulation[34], although the trend has since reversed and surface winds appear to be strengthening[35]. A weak increase in wind speeds has also been detected over the Arctic[20], where it is expected to cause a deepening of the mixed layers as sea ice recedes[19,36]. We find significant regional trends in wind speeds (Fig. 3), where the winds increase the most over the ice-freed Arctic and Southern Ocean, and decrease over the other areas that were not covered by sea ice (supplementary Figs. 3 and 4). Yet at their maximum, both the average and maximum wind speeds change by 2 m s^{-1} over the entire run, or approximately 0.01 m s^{-1} per year, which we argue has a negligible impact on the MLD. As highlighted by ref [20], as a first approximation changes in wind speeds are proportional to changes in MLD, and in observations and models at most the constant of proportionality is 4 s. That is, our change in wind would result in a change in MLD of less than 10 m over the entire run; they represent less than 4% of the MLD trend.

In summary, deep water formation and overall vertical mixing in the ocean decrease worldwide as atmospheric CO_2 concentration increases. This decline is consistent with a global increase in upper ocean stratification, associated with climate-change induced warming and/or freshening of the upper ocean and the year-round disappearance of the sea ice cover. The trends in wind are too weak to be responsible for the projected changes in mixed layer. A decrease in MLD will in turn impact the stratification and the surface heat flux, potentially creating feedback loops. How do these various trends interplay?

The decline in deep water formation is self-reinforcing

The trends in net surface heat flux into the ocean are of opposite sign between the ice-freed and always-ice-free regions, and non negligible (Fig. 3). Somewhat unexpectedly, the increase in ice-free areas as atmospheric temperatures rise results in the ocean gaining heat (or losing less) in the Southern Ocean (supp. Fig 4), as in observations[37], but losing heat over the Arctic. To show that this is in fact consistent with the changes in MLD, we conducted a lagged correlation analysis of our various “CO_2-series”.

Bear in mind that correlation does not mean causation, but it is a strong hint at a physical relationship especially when such relationship has been shown before in different contexts. Regarding the stratification first, we find that with the exception of a few models in the GIN seas and in the Arctic, the correlation between MLD and stratification is negative (Fig. 4, bottom half): the MLD decline is associated with an increase in stratification, which can lead to a further decrease in MLD. The few cases where the MLD decline are associated with a decrease in stratification (Fig. 4, top half) actually show a slight increase in the volume mixed, i.e. the model switches from very deep MLD over a few grid cells to shallower MLD over a larger area. This larger area is what causes the apparent decrease in stratification of the whole region.

The correlation with the heat flux out of the ocean depends on the region considered, as it depends on which water mass is upwelled by the MLD. The most common behaviour is that as stratification increases, so does the heat gained by the ocean, or more specifically, less heat is lost (Fig. 4, bottom left quadrant): the heat stays in the ocean depth below the stratification cap instead of being brought to the surface by deep MLDs and subsequently lost to the atmosphere. The same reasoning applies to the top right quadrant: MLDs are less deep, but still deep enough to reach the comparatively warm waters, which can now go through the halocline to the surface as stratification is reduced. Whether heat is gained or lost by the ocean does not depend only on MLD changes, but also on the temperature difference at the sea surface between the ocean and the atmosphere[37]. Thus, for the same behaviour in MLD and stratification, the ice-freed GIN seas gain heat, while the higher latitude Arctic loses heat. Note that the disappearance of sea ice in itself is responsible for (latent) heat loss, from ice melt and potentially increased evaporation. Finally, a few models in the Arctic and the Southern Ocean increase stratification as the MLD decreases, but lose heat (Fig. 4, bottom right). Most of these models actually exhibit the behaviour described by ref [37], whereby a decline in MLD is associated with larger heat storage but a decrease in net surface heat flux, or more simply: heat is advected away from where there used to be deep MLDs, hence the apparent surface heat loss.

In summary, the evolution of the signal that the ocean sends back to the atmosphere in response to increasing atmospheric CO_2 concentrations is complex. It depends not only on the feedback loop between MLD and stratification, but also on the underlying hydrography and circulation. At the global scale, there is no more open ocean deep convection by 500 – 600 ppm, and it does not re-emerge in the rest of the simulation. Yet some deep water formation continues. In the Southern Ocean, this deep water is most likely formed by shelf processes[38], but our findings can also simply be indicative of the much longer time needed by the Southern Ocean to react to such changes[37]. Recent findings cast doubt on this picture though by showing that the global ocean interior is already exhibiting detectable anthropogenic changes[39]. A cynical reader could also interpret these results as good news: as suggested before[22], with increasing atmospheric CO_2 concentration, models become more accurate as spurious open ocean deep convection disappears from the simulated Southern Ocean. In the North Atlantic, our findings concur with the observed weakening of the AMOC[40]. In fact, it is suspected that deep water formation has already started decreasing; we simply do not have long enough observational records to be certain[41,42,43]. In light of our results, this would not be surprising as sea ice is dramatically decreasing[44] and stratification is increasing in response to surface waters' warming[45] and freshening[21].

Finally, although heat can be transported over large distances by the wind-driven gyres[46], reduced deep water formation means reduced transport of anthropogenic heat and carbon to the deep ocean[2,3], which will accelerate the increase in stratification and in atmospheric CO_2, thus further accelerating the decrease in deep water formation according to our results. Paleoceanographic records show that ultimately, deep mixing would restart[47,48,49]. But in the meantime, as deep water formation has wider impacts than those presented in this text, its sharp decline will most likely worsen the observed drop in oceanic oxygen content[1,4], with potentially dire consequences for the oceanic ecosystem and coastal communities[50].

References

1. Schmidtko, S., Stramma L. & Visbeck M. Decline in global oceanic oxygen content during the past five decades. *Nature* 542, 335 (2017).

2. Ganachaud, A. & Wunsch, C. Improved estimates of global ocean circulation, heat transport and mixing from hydrographic data. *Nature* 408, 453. (2000).

3. Orsi, A. H., Jacobs, S. S., Gordon, A. L. & Visbeck, M. Cooling and ventilating the abyssal ocean. *Geophys. Res. Lett.* 28, 2923-2926. (2001).

4. Marinov, I. et al. Impact of oceanic circulation on biological carbon storage in the ocean and atmospheric pCO2. *Global Biogeochem. Cy.* 22 (2008).

5. Huhn, O., Rhein, M., Hoppema, M. & van Heuven, S. Decline of deep and bottom water ventilation and slowing down of anthropogenic carbon storage in the Weddell Sea, 1984–2011. *Deep Sea Res. Pt I* 76, 66-84. (2013).

6. Medoc Group. Observation of formation of deep water in the Mediterranean Sea, 1969. *Nature* 227, 1037 (1970).

7. Roether, W. et al. (1996). Recent changes in eastern Mediterranean deep waters. *Science* 271, 333-335.

8. Killworth, P. D. Deep convection in the world ocean. *Rev. Geophys.* 21, 1-26. (1983).

9. Marshall, J. & Schott, F. Open-ocean convection: Observations, theory, and models. *Rev. Geophys.* 37, 1-64 (1999).

10. Lab Sea Group. The Labrador Sea deep convection experiment. *B. Am. Meteorol. Soc.* 79, 2033-2058 (1998).

11. Pickart, R. S., Spall, M. A., Ribergaard, M. H., Moore, G. K. & Milliff, R. F. Deep convection in the Irminger Sea forced by the Greenland tip jet. *Nature* 424, 152 (2003).

12. Rudels, B. & Quadfasel, D. Convection and deep water formation in the Arctic Ocean-Greenland Sea system. *J. Marine Syst*. 2, 435-450 (1991).

13. Meincke, J., Rudels, B. & Friedrich, H. J. The Arctic Ocean–Nordic Seas thermohaline system. *ICES J. Mar. Sci.* 54, 283-299 (1997).

14. Kim, K. R. et al. A sudden bottom-water formation during the severe winter 2000–2001: The case of the East/Japan Sea. *Geophys. Res. Lett*. 29, 75-1 (2002).

15. Holliday, N. P., Pollard, R. T., Read, J. F. & Leach, H. Water mass properties and fluxes in the Rockall Trough, 1975–1998. *Deep Sea Res. Pt I* 47, 1303-1332 (2000).

16. Smith Jr, W. O., & Barber D., eds. *Polynyas: windows to the world*. Vol. 74. Elsevier, 2007.

17. Killworth, P. D. On “chimney” formations in the ocean. *J. Phys. Oceanogr.* 9, 531-554. (1979).

18. Ohshima, K. I. et al. Antarctic Bottom Water production by intense sea-ice formation in the Cape Darnley polynya. *Nat. Geosci.* 6, 235 (2013).

19. Lique, C., Johnson, H. L. & Plancherel, Y. Emergence of deep convection in the Arctic Ocean under a warming climate. *Clim. Dyn.* 50, 3833-3847 (2018).

20. Peralta-Ferriz, C. & Woodgate, R. A. Seasonal and interannual variability of pan-Arctic surface mixed layer properties from 1979 to 2012 from hydrographic data, and the dominance of stratification for multiyear mixed layer depth shoaling. *Prog. Oceanogr.* 134, 19-53. (2015).

21. Somavilla, R., González-Pola, C., & Fernández-Diaz, J. The warmer the ocean surface, the shallower the mixed layer. How much of this is true? *J. Geophys. Res.* 122, 7698-7716. (2017).

22. De Lavergne, C., Palter, J. B., Galbraith, E. D., Bernardello, R. & Marinov, I. Cessation of deep convection in the open Southern Ocean under anthropogenic climate change. *Nat. Clim. Change* 4, 278 (2014).

23. Latif, M., Martin, T. & Park, W. Southern Ocean sector centennial climate variability and recent decadal trends. *J. Climate*, 26, 7767-7782 (2013).

24. Wilson, E. A., Riser, S. C., Campbell, E. C., & Wong, A. P. Winter Upper-Ocean Stability and Ice–Ocean Feedbacks in the Sea Ice–Covered Southern Ocean. *J. Phys. Oceanogr.* 49, 1099-1117 (2019).

25. Rind, D. et al. Effects of glacial meltwater in the GISS coupled atmosphere-ocean model: 2. A bipolar seesaw in Atlantic Deep Water production. *J. Geophys. Res*. 106, 27355-27365. (2001).

26. Richardson, G., Wadley, M.R., Heywood, K.J., Stevens, D.P. & Banks, H.T.. Short-term climate response to a freshwater pulse in the Southern Ocean. *Geophys. Res. Lett.* 32 (2005).

27. De Boer, A. M. et al. Interconnectivity between volume transports through Arctic straits. *J. Geophys. Res.* 123, 8714-8729 (2018).

28. Eyring, V. et al. Overview of the Coupled Model Intercomparison Project Phase 6 (CMIP6) experimental design and organization. Geosci. Model Dev. 9, 1937–1958 (2016).

29. Gidden, M. et al. Global emissions pathways under different socioeconomic scenarios for use in CMIP6: a dataset of harmonized emissions trajectories through the end of the century. *Geosci. Model Dev*. 12, 1443-1475 (2019).

30. Heuzé, C., 2020. Antarctic Bottom Water and North Atlantic Deep Water in CMIP6 models. *Ocean Sci. Discuss.* (2020).

31. SIMIP Community. Arctic Sea Ice in CMIP6. *Geophys. Ress Lett*. 47 (2020).

32. Roach, L.A., Dörr, J., Holmes, C.R., Massonnet, F., Blockley, E.W., Notz, D., Rackow, T., Raphael, M.N., O'Farrell, S.P., Bailey, D.A. & Bitz, C.M. Antarctic sea ice area in CMIP6. *Geophys. Res. Lett.*, 47 (2020)

33. IPCC, 2014: Climate Change 2014: Synthesis Report. Contribution of Working Groups I, II and III to the Fifth Assessment Report of the Intergovernmental Panel on Climate Change [Core Writing Team, R.K. Pachauri and L.A. Meyer (eds.)]. IPCC, Geneva, Switzerland, 151 pp

34. Vautard, R., Cattiaux, J., Yiou, P., Thépaut, J.N. & Ciais, P. Northern Hemisphere atmospheric stilling partly attributed to an increase in surface roughness. *Nature Geosci*. 3, 756-761 (2010).

35. Zeng, Z., Ziegler, A.D., Searchinger, T., Yang, L., Chen, A., Ju, K., Piao, S., Li, L.Z., Ciais, P., Chen, D. & Liu, J. A reversal in global terrestrial stilling and its implications for wind energy production. *Nature Climate Change* 9, 979-985 (2019).

36. Martin, T., Steele, M. & Zhang, J. Seasonality and long-term trend of Arctic Ocean surface stress in a model. *J. Geophys. Res.* 119, 1723-1738 (2014).

37. Armour, K.C., Marshall, J., Scott, J.R., Donohoe, A. & Newsom, E.R. Southern Ocean warming delayed by circumpolar upwelling and equatorward transport. *Nature Geosci.* 9, 549-554 (2016).

38. Heywood, K.J., Schmidtko, S., Heuzé, C., Kaiser, J., Jickells, T.D., Queste, B.Y., Stevens, D.P., Wadley, M., Thompson, A.F., Fielding, S. & Guihen, D. Ocean processes at the Antarctic continental slope. *Phil. Trans. Royal Soc.* A. 372 (2014).

39. Silvy, Y., Guilyardi, E., Sallée, J.B. & Durack, P.J.. Human-induced changes to the global ocean water masses and their time of emergence. *Nature Climate Change*, 1-7. (2020).

40. Caesar, L., Rahmstorf, S., Robinson, A., Feulner, G. & Saba, V. Observed fingerprint of a weakening Atlantic Ocean overturning circulation. *Nature* 556, 191-196 (2018).

41. Broecker, W. S., Sutherland, S., & Peng, T. H. A possible 20th-century slowdown of Southern Ocean deep water formation. *Science* 286, 1132-1135 (1999).

42. Rahmstorf, S. et al. Exceptional twentieth-century slowdown in Atlantic Ocean overturning circulation. *Nature Clim. Change* 5, 475 (2015).

43. Lozier, M. S. et al. A sea change in our view of overturning in the subpolar North Atlantic. *Science* 363, 516-521 (2019).

44. Notz, D. & Stroeve, J. Observed Arctic sea-ice loss directly follows anthropogenic CO2 emission. *Science* 354, 747-750 (2016).

45. Coma, R. et al. Global warming-enhanced stratification and mass mortality events in the Mediterranean. *PNAS* 106, 6176-6181 (2009).

46. Årthun, M., Eldevik, T. & Smedsrud, L.H., 2019. The role of Atlantic heat transport in future Arctic winter sea ice loss. *J. Climate* 32, 3327-3341 (2019).

47. De Boer, A. M., Sigman, D. M., Toggweiler, J. R., & Russell, J. L. Effect of global ocean temperature change on deep ocean ventilation. *Paleoceanography* 22 (2007).

48. Skinner, L. C. et al. North Atlantic versus Southern Ocean contributions to a deglacial surge in deep ocean ventilation. *Geology* 41, 667-670 (2013).

49. Labeyrie, L. D., Duplessy, J. C. & Blanc, P. L. Variations in mode of formation and temperature of oceanic deep waters over the past 125,000 years. *Nature* 327, 477 (1987).

50. Stramma, L. et al. Expansion of oxygen minimum zones may reduce available habitat for tropical pelagic fishes. *Nature Clim. Change* 2, 33 (2012).

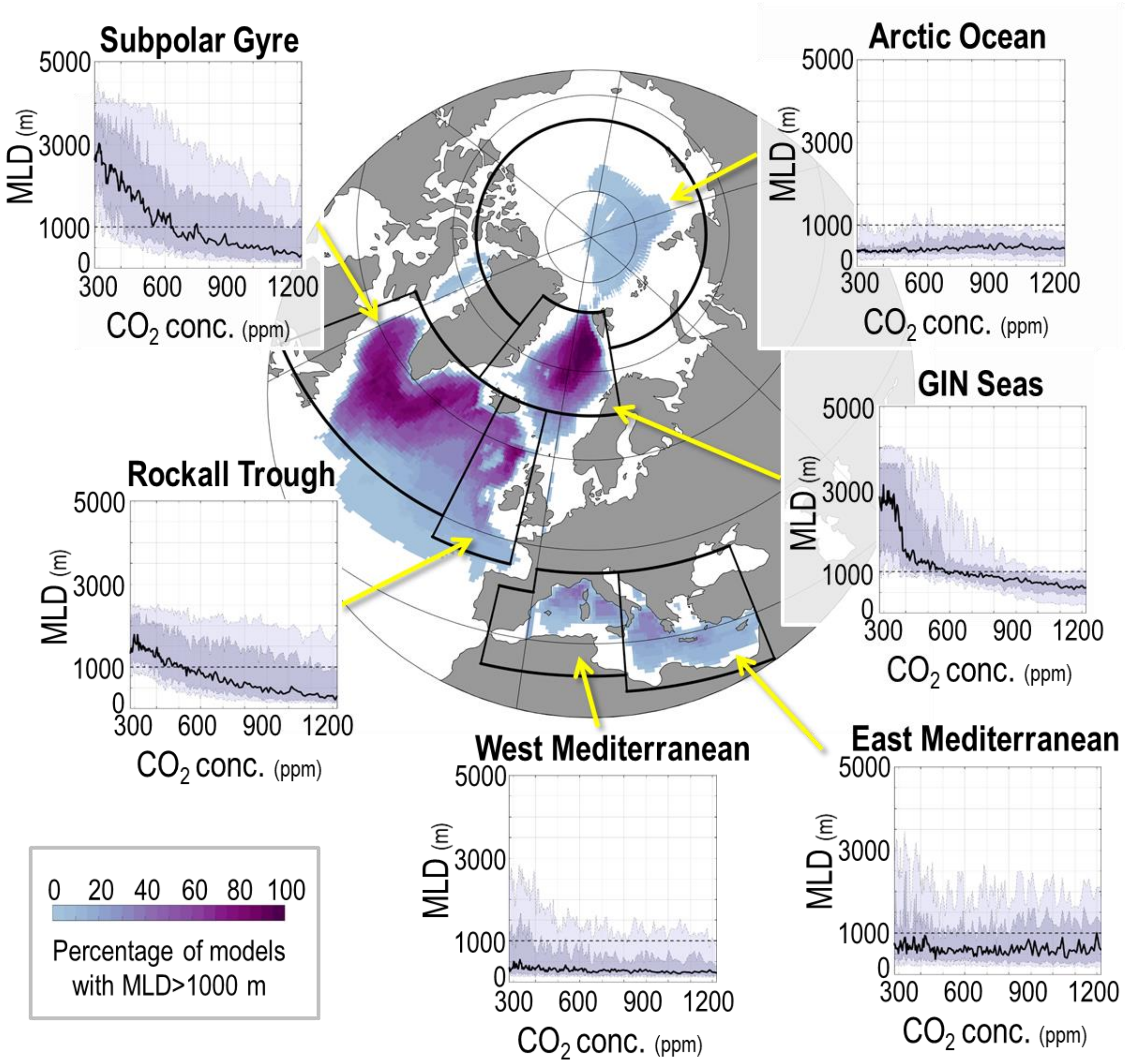

Figure 1 | Hotspots of deep convection in the wider North Atlantic in CMIP6 models. Shaded map shows at each grid point the percentage of models that ever reach a mixed layer depth (MLD) deeper than 1000 m. Inserts show the evolution of this mixed layer depth in each region, delimited by black contours, as atmospheric CO_2 concentration increases: thick black line is the multi model median; dark shading, where 75% of the models are found (interquartile range); light shading, where 90% of the models are found (interdecile range). The spatial pattern of deep water formation corresponds to that observed and/or expected in the real North Atlantic and Mediterranean. For most models, MLDs no longer exceed 1000 m after 600 ppm: deep convection ceases.

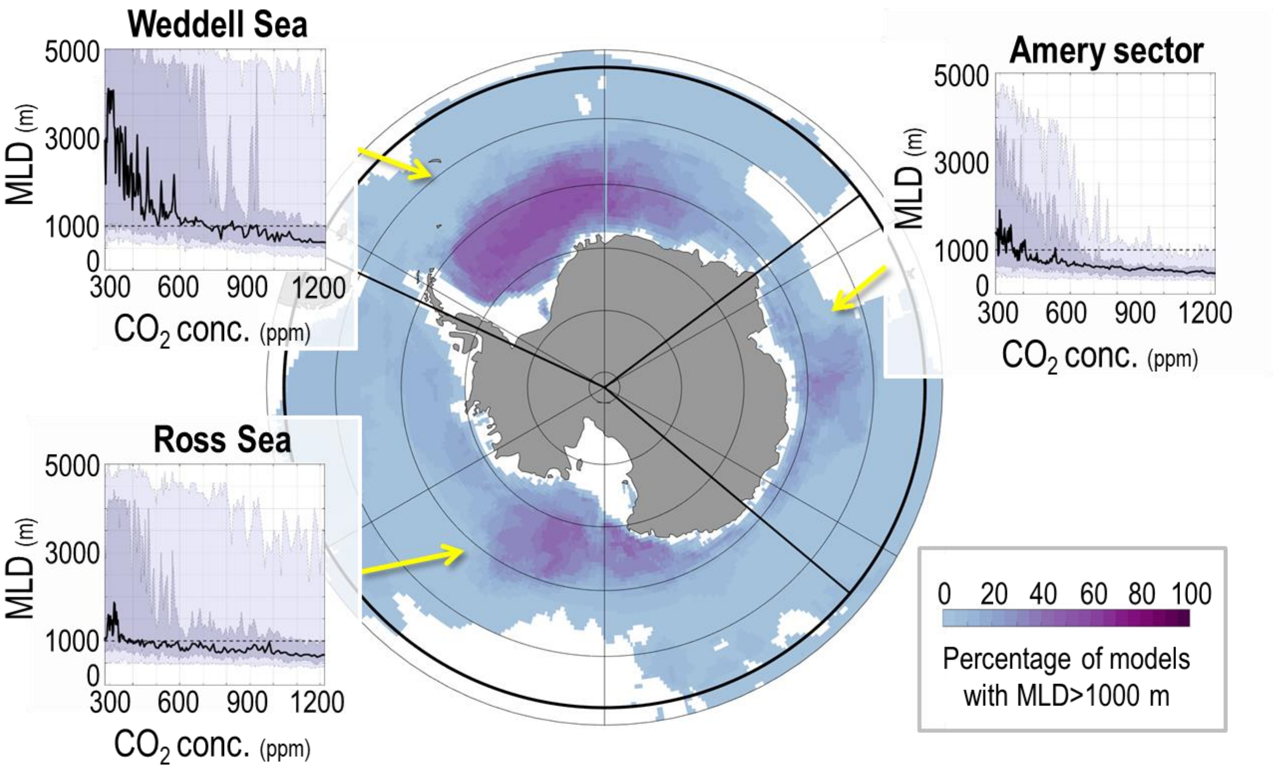

Figure 2 | Hotspots of deep convection in the Southern Ocean in CMIP6 models. Shaded map shows at each grid point the percentage of models that ever reach a mixed layer depth (MLD) deeper than 1000 m. Inserts show the evolution of this mixed layer in each region, delimited by black contours, as atmospheric CO_2 concentration increases: thick black line is the multi model median; dark shading, where 75% of the models are found (interquartile range); light shading, where 90% of the models are found (interdecile range). At historical levels of CO_2, CMIP6 models exhibit spurious open ocean deep convection too often, over too large areas[30]. Mixed layers drastically shoal with increasing CO_2, so for concentrations higher than 400 ppm in the Amery and Ross sectors, and 600 ppm in the Weddell Sea, there is no more (spurious) open ocean deep convection.

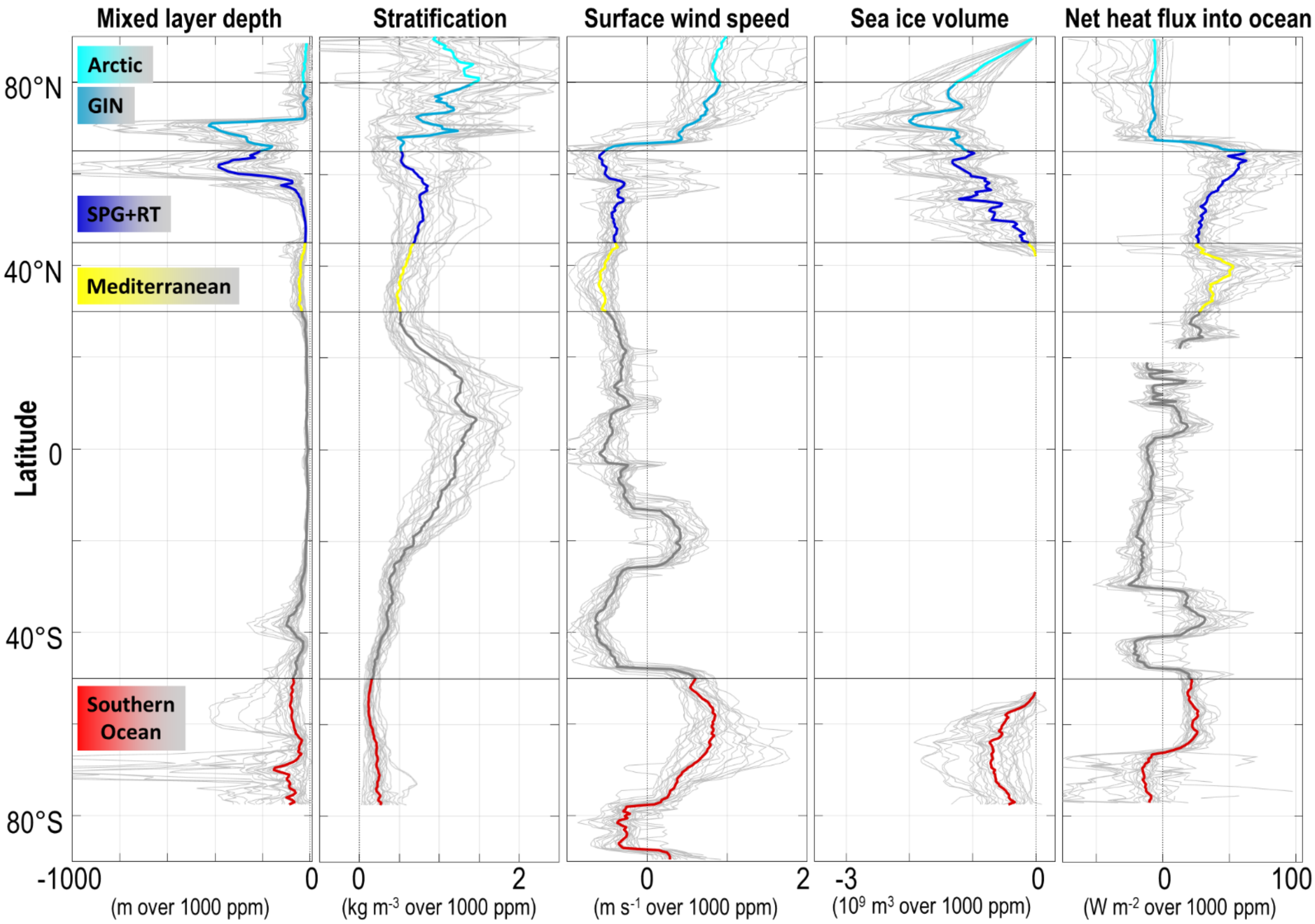

Figure 3 | Trends in mixed layer depth, stratification, wind, sea ice and heat flux. Zonally-averaged trend for each model (thin grey line) and multi-model mean trend (thick, coloured) in mixed layer depth, upper 200 m ocean stratification, surface wind speed, sea ice volume, and net heat flux into the ocean (negative: ocean loses heat; positive, ocean gains heat) as a function of the atmospheric CO_2 concentration in parts per million. Over the length of the run used in this study, the CO_2 concentration increases from 275 ppm to 1225 ppm. Trends are averaged over all longitudes, hence the low values; we indicate the regions of Figs 1 and 2 for comparison purposes only. As seen on Figs 1 and 2, mixed layer depths decrease globally. Stratification increases globally. The trends in wind are too weak to significantly impact the MLD. The combination of changing MLD and sea ice disappearance has region-specific effects on the heat flux – see Main text. See also the corresponding maps in supplementary Figs 3 and 4.

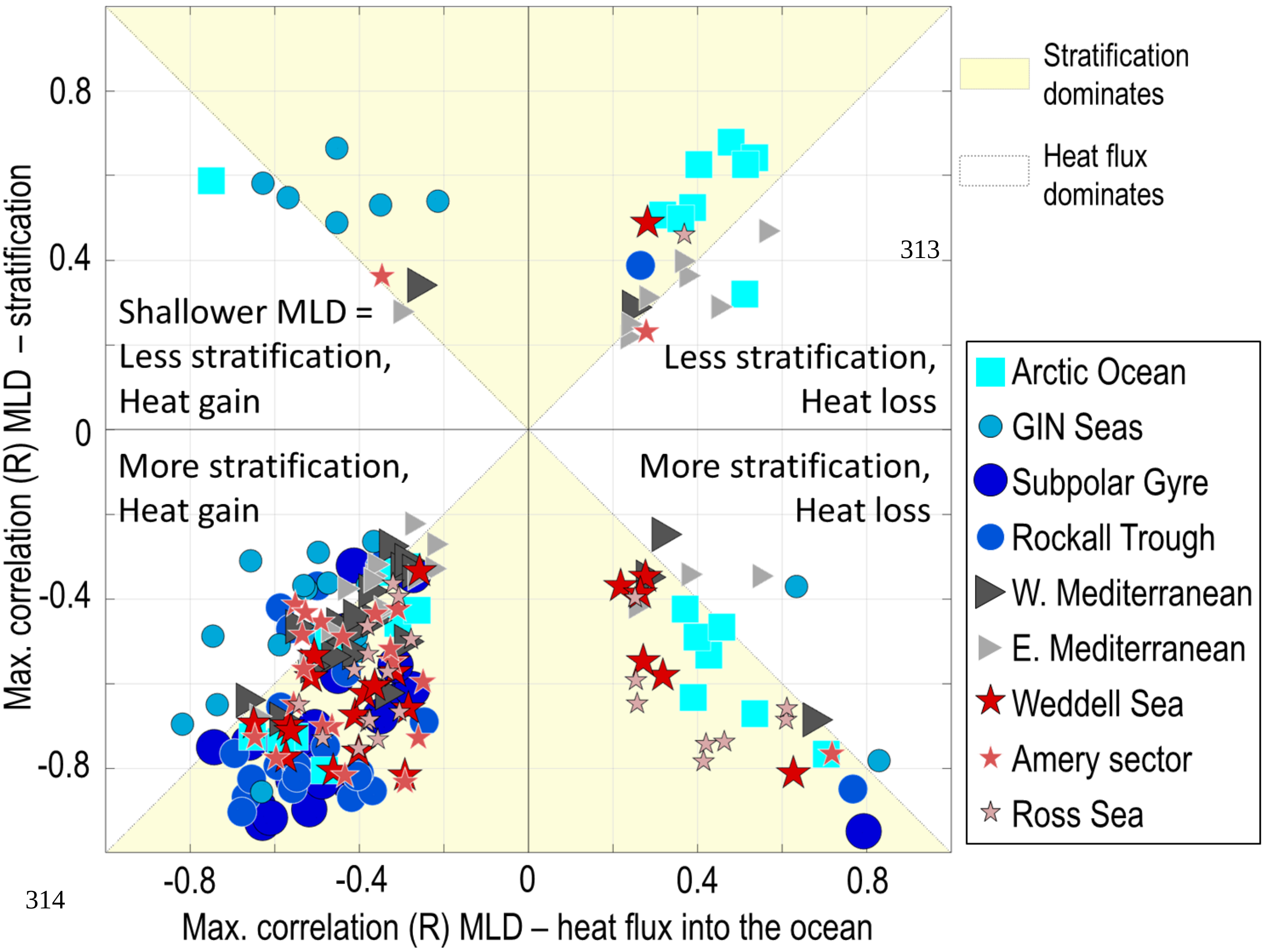

Figure 4 | The shoaling of mixed layer depths is self-reinforcing. Allowing for a lag of up to 300 ppm (see Methods), maximum correlation between mixed layer depths (MLD) and heat flux into the ocean (x-axis) or stratification (y-axis), with MLD coming first, where each symbol represents a different region and each point a model with a significant correlation in that region. For each quadrant, we reformulate these pairs of correlations in terms on their possible association with the dramatic decrease in MLD showed by all previous figures.

Online-only methods for
"Global decline of deep water formation with increasing atmospheric CO_2"

CMIP6 models:

We used 30 models that submitted their monthly output of:

- ocean salinity ('so');
- ocean potential temperature ('thetao');
- sea ice volume per surface area ('sivol') or sea ice mass per surface area ('simass') or sea ice thickness and area fraction ('sithick' and 'siconc');
- and surface wind speed ('sfcWind') or eastward and northward components of the surface wind speed ('uas' and 'vas');

for the so-called 1pctCO2 run of the Climate Model Intercomparison Project phase 6 (CMIP6[1]), listed in supplementary Table 1. We used one ensemble member, r1i1p1f1, as it was the only one for which all models had provided data. If available, we also obtained their mixed layer depth 'mlotst'; otherwise, we computed it as detailed later. The net heat flux into the ocean 'hfds' was obtained when available but not computed otherwise.

In the 1pctCO2 run, the atmospheric CO_2 concentration increases by 1% every year over 150 years from its 1850 value of 275 ppm, reaching over 1200 ppm at the end[1]. As the accuracy of these models with respects to global deep water formation has recently been determined by ref [2], we provide no such assessment here and instead concentrate on the relationship between deep water formation and rising atmospheric CO_2 concentrations, and link the results to projected CO_2 concentrations for the 21st century[1,3]. In the core of the manuscript, for clarity, we refer to the 1pctCO2 run as "one percent CO_2".

The nine regions studied here:

As studies on previous generations of CMIPs have shown that CMIP models regularly exhibit deep water formation in the vicinity and/or over a larger area than in observations[4,5,6,7], we base our region definition here on the multimodel maximum mixed layer depth, and name each region after its equivalent in observations. We obtained ten wide regions, where at least one CMIP6 model maximum MLD ever reaches more than 1000 m depth: the nine regions shown on Figs. 1 and 2, and the East Sea / Sea of Japan in the North Pacific. As this last region is connected to the rest of the world ocean by narrow straits shallower than 200 m depth, and to keep the overall story simple, we chose to exclude it from this study.

Mixed layers and deep water formation:

In the literature, one considers that deep water formation is occurring if the mixed layer depth (MLD) exceeds a critical depth, usually 1000 m[8,9] or even 2000 m in the Southern Ocean[10]. Such binary definition is problematic for two reasons:

1. what happens to the MLD after it becomes shallower than 1000 m is still interesting, as the maximum depth has large climatic impacts depending on the water mass that is reached;
2. several deep water masses are formed by cascading[11], i.e. they do not require very deep mixed layers at one location.

Instead, we computed and present for each year and each region the maximum MLD with no threshold criterion. We also computed the yearly maximum mixed volume for each region as the sum of the mixed layer depth multiplied by the grid cell area for each grid cell of the region. By doing so, we can verify whether the region changes from a few grid cells with very deep MLD to a larger area with shallower MLD.

For robustness, we also computed the global volumes of deep and bottom water produced from the models' meridional ocean velocity 'vo'. Supplementary Figure 1 shows the Atlantic Meridional Overturning Circulation (AMOC) at 35°N as in refs [2,12] and the sum of the Southern Meridional Overturning Circulations at 30°S into the Atlantic, Indian and Pacific oceans as in ref [2]. We present these in Sverdrups, where 1 Sv = 1 million m^3 s^{-1}. Finally, we computed the Atlantic Ocean and global meridional overturning streamfunctions in density coordinates and similarly obtained the volumes of North Atlantic Deep Water and Antarctic Bottom Water as the dense maxima north of 20°N and south of 60°S, respectively.

Note that in this manuscript, in line with previous publications on this topic[4,6,9,10], we make no distinction between deep mixed layers, deep mixing and deep convection.

Derived variables: volumes, stratification, and properties of the mixed layer

For each model, for each month and each grid cell, we also computed:

- when 'mlotst' was not available, the mixed layer depth using the same definition as for 'mlotst': the depth where σ_θ differs by more than 0.125 kg m^{-3} than that at 10 m depth, and where σ_θ was obtained from 'so' and 'thetao';
- the sea ice volume in m^3, defined as the sea ice volume per surface area 'sivol', multiplied by the grid cell area. If 'sivol' was not available, we either computed it from 'simass' by dividing it by the ice density used by CMIP6 (900 kg m^{-3}), or by multiplying the sea ice thickness 'sithick' by the sea ice concentration 'siconc';
- the potential temperature and salinity of the mixed layer, defined as the median from the ocean surface to the MLD of the ocean potential temperature 'thetao' and ocean salinity 'so'

respectively. Throughout the manuscript, we will refer to the potential temperature as "the temperature" only;

– the ocean stratification.

There are at least two definitions for the stratification in the literature: the difference in potential density between 1) the surface and 200 m depth[13], or 2) the last depth level inside the mixed layer and the first level outside of it[14]. We computed both. For all the models and all the regions, both definitions yielded similar trends and similar correlations (not shown). For consistency among all the models, among all the regions, and throughout the run, but also to improve the readability, we chose to present only the stratification based on the fixed depth level of 200 m.

We computed region averages of these properties, the wind speed 'sfcWind' and the net heat flux 'hfds' using 1) only the individual grid cells where the maximum MLD over the entire run exceeds 1000 m; and 2) all the grid cells in a region. Again, both options yielded similar results, but in order to present consistent comparisons between the models, regions and CO_2 concentrations, we show only the values obtained with option 2 (all the grid cells of a given region).

Trends:

To determine the (potential) relationship between an increase in atmospheric CO_2 and changes in deep water formation, as well as relationships with the suspected drivers of deep water formation and its impact, linear and logarithmic trends as a function of the CO_2 concentration were determined for each parameter. The significance of each trend at the 95% confidence level was verified with both a Student's t-test and Pearson correlations. We present the results of the second method only as the number of degrees of freedom for the Student's t-test, i.e. possible autocorrelations within each parameter series, is model-, region- and even parameter-dependent. Finally, each trend was also visually validated.

We present only the linear trends for three reasons: 1) the linear and logarithmic trends are similar (not shown); 2) the values of the linear trends are more intuitive to understand than the logarithmic ones; 3) from visual comparison, the linear trends actually are conservative estimates of the dramatic declines.

In the core of the text, we present only the multi model average of the significant trends along with the models' agreement regarding the sign of these trends. These averages are not weighted.

Lagged correlations:

To try and find potential relationships between changes in deep water formation and changes in wind speed, sea ice volume, stratification or heat flux, we computed the lagged correlation between these parameters with a lag in time of up to 50 years both ways, and a lag in atmospheric CO_2 concentration of up to 300 ppm, which in both cases corresponds to roughly 1/3 of the signal length. Only correlations that are significant at the 95% level are considered.

Data availability:

The CMIP6 datasets analysed during the current study are publicly available online through the Earth System Grid Federation (ESGF). We mostly used the data made available on the Lawrence Livermore National Laboratory node: https://esgf-node.llnl.gov, occasionally completed by the Institut Pierre Simon Laplace node: https://esgf-node.ipsl.upmc.fr.

Code availability:

The codes written for the current study are available on request.

References for the methods:

1. Eyring, V., et al. Overview of the Coupled Model Intercomparison Project Phase 6 (CMIP6) experimental design and organization. *Geosci. Model Dev.* 9, 1937–1958 (2016).

2. Heuzé, C., 2020. Antarctic Bottom Water and North Atlantic Deep Water in CMIP6 models. *Ocean Sci.Discuss.* (2020)

3. O'Neill, B.C., et al. The Scenario Model Intercomparison Project (ScenarioMIP) for CMIP6. *Geosci. Model Dev.*, 9, 3461–3482 (2016).

4. Heuzé, C., Heywood, K.J., Stevens, D.P., & Ridley, J.K. Southern Ocean bottom water characteristics in CMIP5 models. *Geophys. Res. Lett.*, 40, 1409-1414 (2013).

5. Sallée, J-B., et al. Assessment of Southern Ocean mixed-layer depths in CMIP5 models: Historical bias and forcing response. *J. Geophys. Res. Oceans*, 118, 1845-1862 (2013).

6. Heuzé, C. North Atlantic deep water formation and AMOC in CMIP5 models. *Ocean Sci.*, 13, 609-622 (2017).

7. Menary, M.B., et al. Exploring the impact of CMIP5 model biases on the simulation of North Atlantic decadal variability. *Geophys. Res. Lett.* 42, 5926-5934 (2015).

8. Brodeau, L. & Koenigk, T.: Extinction of the northern oceanic deep convection in an ensemble of climate model simulations of the 20th and 21st centuries, Climate Dynamics, 46 (2016).

9. Våge, K., et al. Surprising return of deep convection to the subpolar North Atlantic Ocean in winter 2007–2008. *Nat. Geosci*. 2, 67 (2009).

10. de Lavergne, C., Palter, J.B., Galbraith, E.D., Bernardello, R., & Marinov, I.. Cessation of deep convection in the open Southern Ocean under anthropogenic climate change. Nature Climate Change, 4, 278 (2014).

11. Ivanov, V.V., Shapiro, G.I., Huthnance, J.M., Aleynik, D.L. & Golovin, P.N. Cascades of dense water around the world ocean. *Progress in oceanography*, 60 (2004)

12. Menary, M.B., Robson, J., Allan, R., Booth, B.B., Cassou, C., Gastineau, G., Gregory, J., Hodson, D., Jones, C., Mignot, J. & Ringer, M. Aerosol-forced AMOC changes in CMIP6 historical simulations. *Geophysical Research Letters* (2020)

13. Capotondi, A., Alexander, M.A., Bond, N.A., Curchitser, E.N., & Scott, J.D.. Enhanced upper ocean stratification with climate change in the CMIP3 models. *J. Geophys. Res. Oceans* 117, C4 (2012).

14. Peralta-Ferriz, C., & Woodgate, R.A. "Seasonal and interannual variability of pan-Arctic surface mixed layer properties from 1979 to 2012 from hydrographic data, and the dominance of stratification for multiyear mixed layer depth shoaling." *Prog. Oceanogr.* 134, 19-53 (2015).

Supplementary material for

"Global decline of deep water formation with increasing atmospheric CO_2"

Model name	MLD	Sea ice	Wind	hfds	Ref.
ACCESS-CM2	mlotst	sivol	sfcWind	x	N/A
ACCESS-ESM1-5	mlotst	sivol	sfcWind	x	1
BCC-CSM2-MR	mlotst	sivol	sfcWind		2
BCC-ESM1	mlotst	sivol	sfcWind		2
CAMS-CSM1-0	mlotst	sivol	sfcWind	x	3
CanESM5	mlotst	simass	sfcWind	x	4
CESM2	mlotst	sivol	sfcWind	x	5
CESM2-WACCM	mlotst	sivol	sfcWind	x	5
CMCC-CM2-SR5	mlotst	sivol	sfcWind	x	6
CNRM-CM6-1	mlotst	sivol	sfcWind	x	7
CNRM-ESM2-1	mlotst	sivol	sfcWind	x	8
EC-Earth3-Veg	mlotst	sivol	sfcWind	x	9
GFDL-CM4	we compute	sivol	sfcWind	x	10
GFDL-ESM4	we compute	sivol	sfcWind	x	N/A
GISS-E2-1-G	mlotst	sivol	sfcWind	x	11
GISS-E2-1-H	we compute	sivol	sfcWind	x	11
GISS-E2-2-G	mlotst	sivol	sfcWind	x	12
HadGEM3-GC31-LL	mlotst	sivol	sfcWind	x	13
IPSL-CM6A-LR	mlotst	sivol	sfcWind	x	14
MCM-UA-1-0	we compute	sithick	uas+vas	x	N/A
MIROC-ES2L	we compute	sithick+siconc	sfcWind		15
MIROC6	we compute	simass	sfcWind		16
MPI-ESM1-2-HR	mlotst	sivol	sfcWind	x	17
MPI-ESM1-2-LR	mlotst	sivol	sfcWind	x	18
MRI-ESM2-0	we compute	sivol	sfcWind	x	19
NESM3	mlotst	sithick+siconc	uas+vas	x	20
NorESM2-LM	mlotst	sivol	sfcWind	x	21
NorESM2-MM	mlotst	sivol	sfcWind	x	21
SAM0-UNICON	we compute	sivol	sfcWind	x	22
UKESM1-0-LL	mlotst	sivol	sfcWind	x	23

Supplementary Table 1 | The 30 models used for this study. For each model, we indicate their CMIP6 name; whether the mixed layer depth was available as the output 'mlotst' or we had to compute it from the ocean temperature and salinity; which sea ice output was available ('sivol' is the sea ice volume divided by cell area; 'simass', the mass; 'sithick', the thickness; and 'siconc', the concentration); which wind output was available ('sfcWind' the wind speed at the sea surface; 'uas' and 'vas' the sea surface zonal and meridional wind components respectively); whether the net heat flux output 'hfds' was available; and the corresponding reference when available, provided at the end of this document.

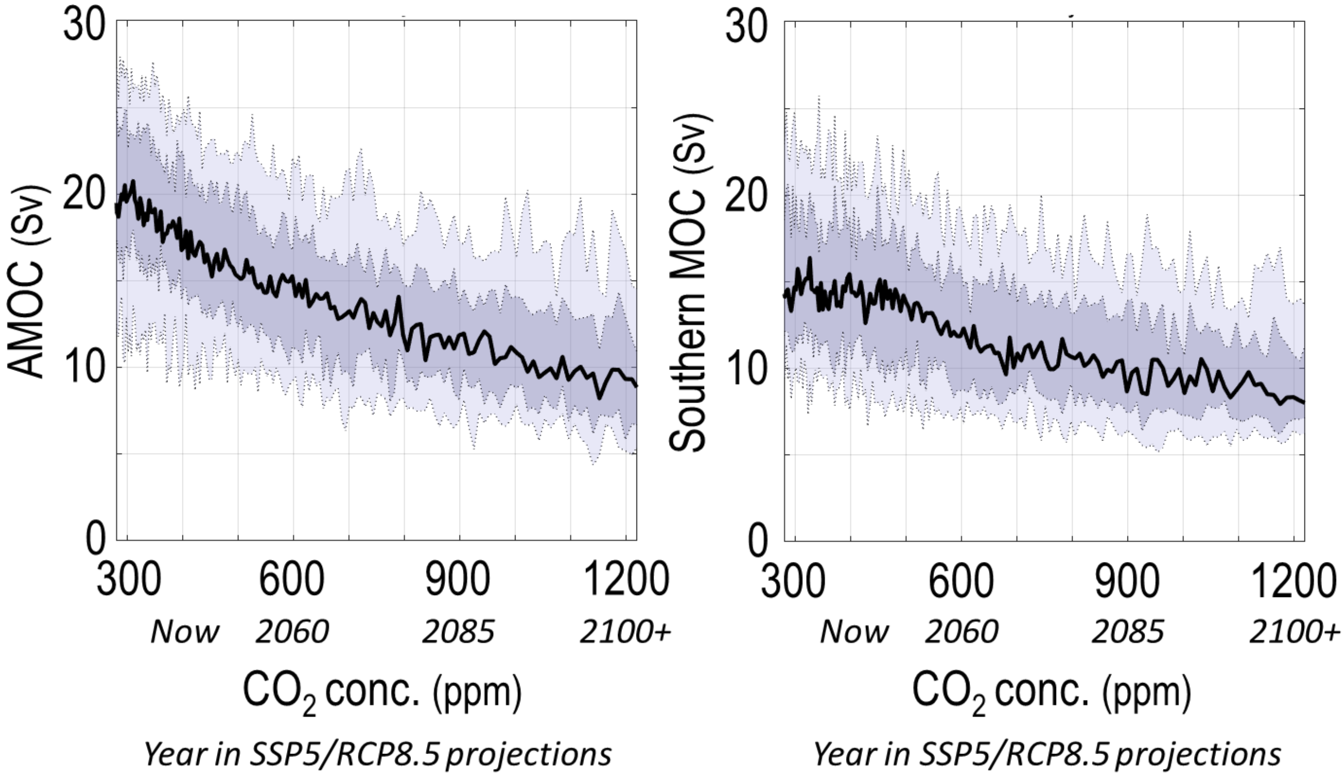

Supplementary Figure 1 | Deep water formation is at least halved. Weakening of the Atlantic Meridional Overturning Circulation (AMOC) at 35°N and the Southern MOC at 30°S (computed as in ref [24], in Sverdrups where 1 Sv = 10^6 m^3 s^{-1}) in response to increasing atmospheric CO_2 concentrations. These series are consistent with the strong decrease in mixed layers in both the North Atlantic and Southern Ocean regions (Figs 1 and 2). Similar results were obtained from the overturning streamfunction in density coordinates (not shown).

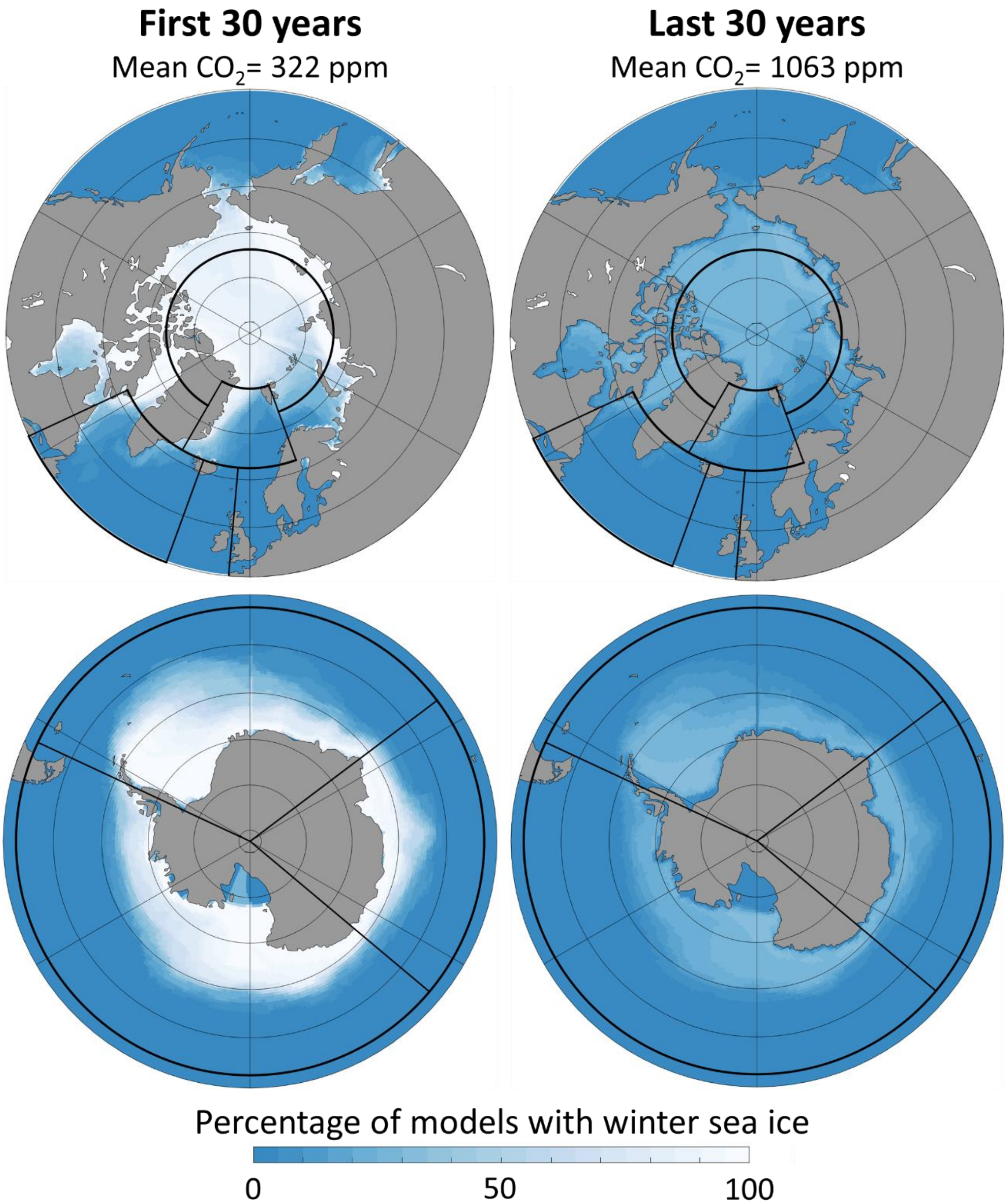

Supplementary Figure 2 | Winter sea ice has disappeared at the end of the simulation. Percentage of models with a non-zero winter sea ice volume for each grid cell for the first thirty years of the one percent CO_2 simulation (left, mean of 322 ppm) and the last thirty years (right, mean of 1063 ppm) in the northern and southern hemispheres. Black lines are identical to those of Figs 1 and 2 and highlight the region definition. Most models have no more sea ice even in winter at high CO_2 levels (corresponding to the end of the 21st century).

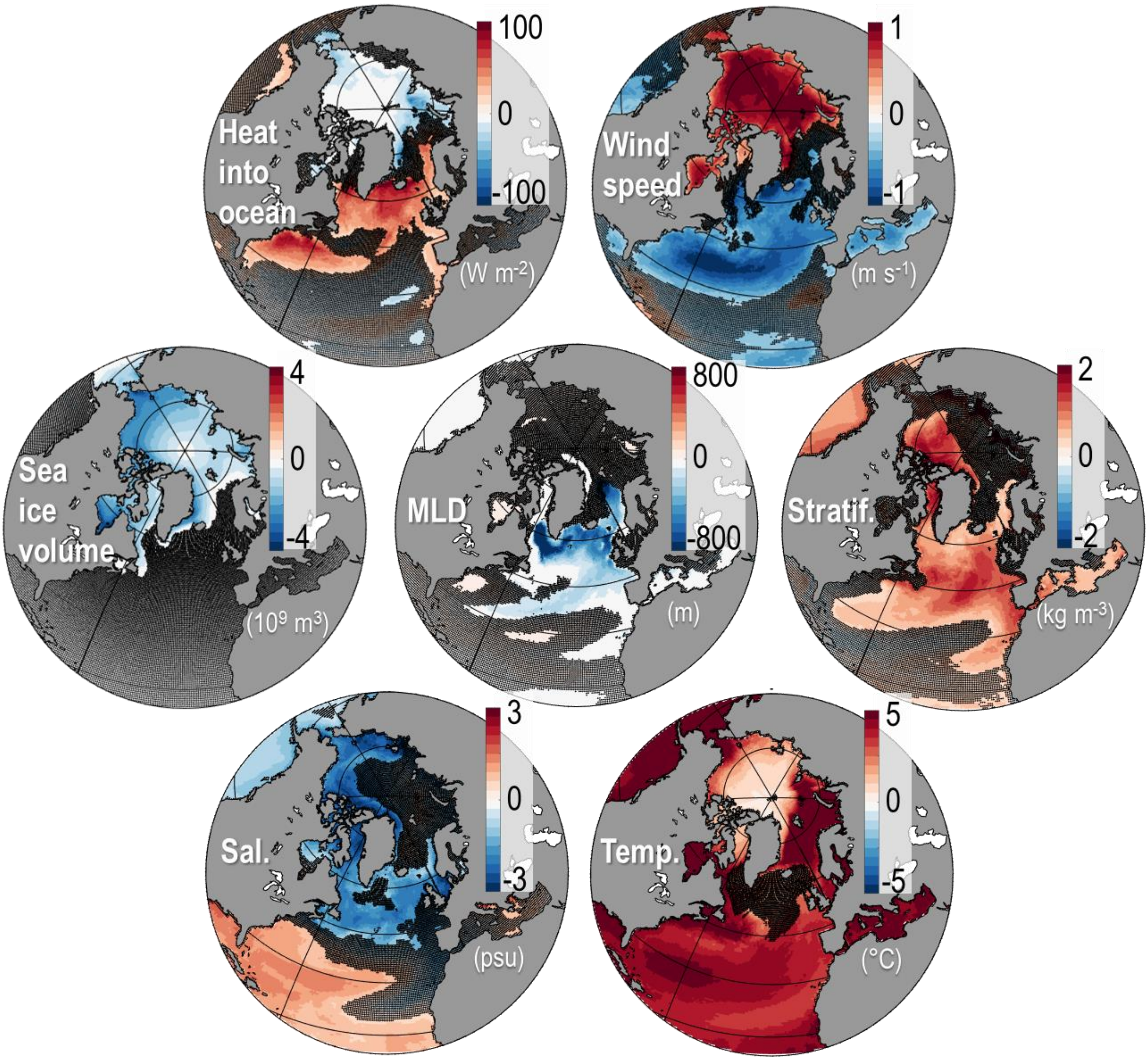

Supplementary Figure 3 | In the North Atlantic, the trends depend on the region considered. Multimodel median linear trends in net heat flux into the ocean (positive means heat gained / less heat lost by the ocean), surface wind speed, sea ice volume, mixed layer depth (MLD), upper 200 m ocean stratification (Stratif.), and salinity (Sal.) and temperature (Temp.) of the mixed layer, as a function of the atmospheric CO2 concentration in parts per million (ppm). Over the length of the run used in this study, the CO2 concentration increases from 275 ppm to 1225 ppm, so as per Fig. 3 we here give the trend over 1000 ppm. Hatching indicates that less than 66% of the models agree on the sign of the trend. Heat flux, wind and temperature differ between the regions that are losing their ice and those that always were ice free. The salinity increases at low latitude but decreases elsewhere. MLD decreases and stratification increases overall.

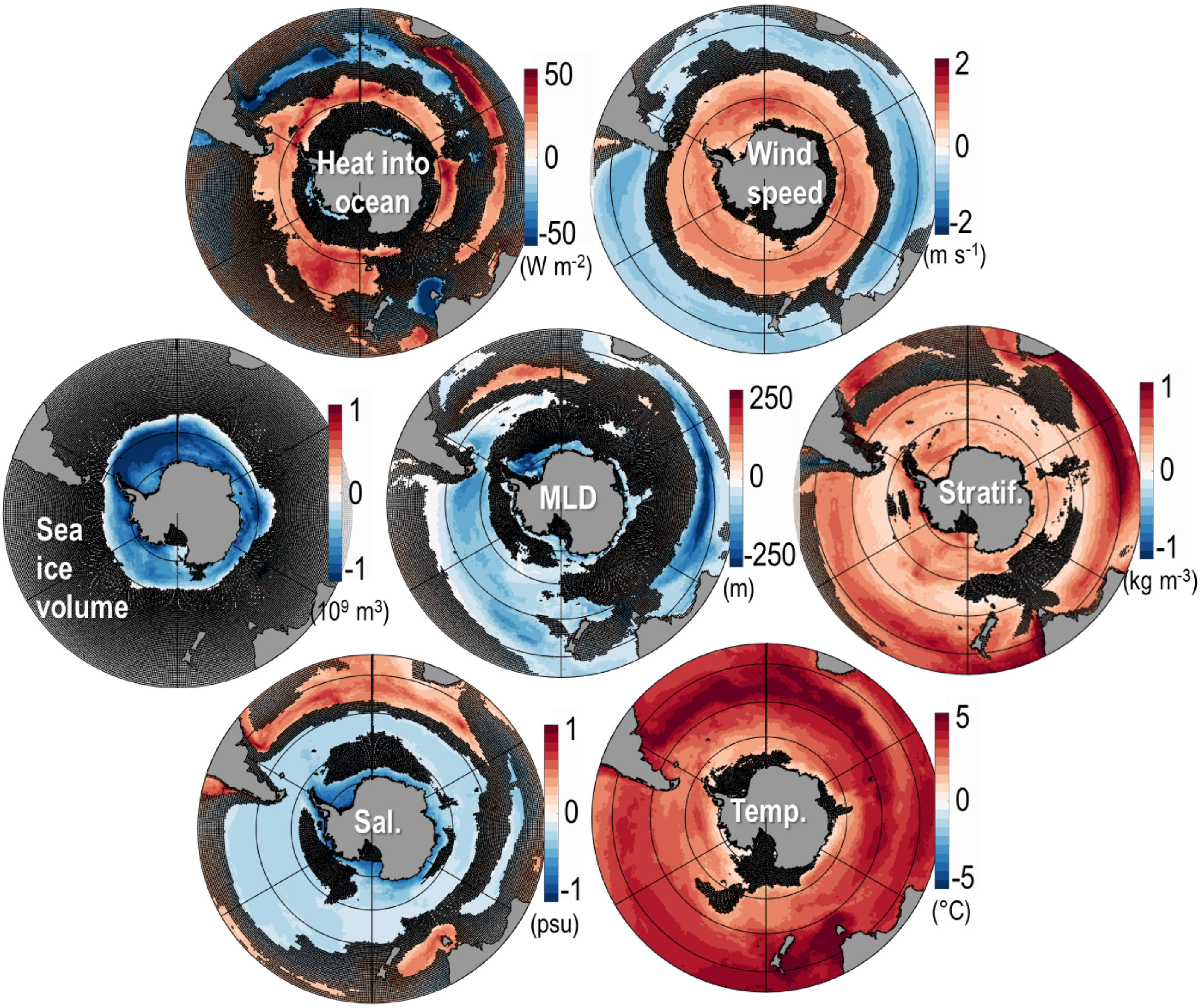

Supplementary Figure 4 | In the Southern Ocean, the trends are mostly zonal. Same legend as supplementary Figure 3. In the Southern Ocean, trends are zonal and differ most on either side of the Polar Front, with an increase in heat and wind, and decrease in MLD and salinity south of it (roughly south of 40°S), and a decrease in heat and wind but strong increase in stratification, salinity and temperature north of it. The lack of multimodel agreement close to the continent reflects the diversity of the models' locations of open ocean deep convection.

Supplementary references

1. Ziehn, T., Lenton, A., Law, R. M., Matear, R. J., & Chamberlain, M. The carbon cycle in the Australian Community Climate and Earth System Simulator (ACCESS-ESM1)-Part 2: Historical simulations, *Geoscientific Model Development*, 10 (2017)

2. Wu, T. et al. The Beijing Climate Center Climate System Model (BCC-CSM): the main progress from CMIP5 to CMIP6, *Geoscientific Model Development*, 12 (2019)

3. Rong, X. Y., Li, J., & Chen, H. M. Introduction of CAMS-CSM model and its participation in CMIP6, *Climate Change Res*, 6 (2019)

4. Swart, N., et al. The Canadian Earth System Model version 5 (CanESM5. 0.3), *Geoscientific Model Development*, 12 (2019)

5. Danabasoglu, G., et al. The Community Earth System Model version 2 (CESM2), *Journal of Advances in Modeling Earth Systems*, 12 (2020)

6. Cherchi, A., et al. Global Mean Climate and Main Patterns of Variability in the CMCC-CM2 Coupled Model. *Journal of Advances in Modeling Earth Systems*, 11 (2019)

7. Voldoire, A. et al. Evaluation of CMIP6 DECK Experiments with CNRM-CM6-1, *Journal of Advances in Modeling Earth Systems*, 11 (2019)

8. Séférian, R., Nabat, P., Michou, M., Saint-Martin, D., Voldoire, A., Colin, J., Decharme, B., Delire, C., Berthet, S., Chevallier, M., & Sénési, S.: Evaluation of CNRM Earth System Model, CNRM-ESM2-1: Role of Earth System Processes in Present-Day and Future Climate, *Journal of Advances in Modeling Earth Systems*, 11 (2019)

9. Wyser, K., Kjellström, E., Koenigk, T., Martins, H. & Döscher, R.. Warmer climate projections in EC-Earth3-Veg: the role of changes in the greenhouse gas concentrations from CMIP5 to CMIP6. *Environmental Research Letters*, 15 (2020)

10. Held, I., Guo, H., Adcroft, A., Dunne, J., Horowitz, L., Krasting, J., Shevliakova, E., Winton, M., Zhao, M., Bushuk, M., & Wittenberg, A. Structure and performance of GFDL's CM4.0 climate model, *Journal of Advances in Modeling Earth Systems*, 11 (2019)

11. Kelley, M., Schmidt, G.A., Nazarenko, L.S., Bauer, S.E., Ruedy, R., Russell, G.L., Ackerman, A.S., Aleinov, I., Bauer, M., Bleck, R. & Canuto, V. GISS-E2. 1: Configurations and Climatology. *Journal of Advances in Modeling Earth Systems*, 11 (2019).

12. Rind, D., Orbe, C., Jonas, J., Nazarenko, L., Zhou, T., Kelley, M., Lacis, A., Shindell, D., Faluvegi, G., Romanou, A. & Russell, G., 2020. GISS Model E2. 2: A Climate Model Optimized for the Middle Atmosphere—Model Structure, Climatology, Variability, and Climate Sensitivity. *Journal of Geophysical Research: Atmospheres*, 125 (2020)

13. Kuhlbrodt, T., Jones, C., Sellar, A., Storkey, D., Blockley, E., Stringer, M., Hill, R., Graham, T., Ridley, J., Blaker, A., & Calvert, D.: The low-resolution version of HadGEM3 GC3. 1: Development and evaluation for global climate, *Journal of Advances in Modeling Earth Systems*, 10 (2018)

14. Lurton, T., Balkanski, Y., Bastrikov, V., Bekki, S., Bopp, L., Braconnot, P., Brockmann, P., Cadule, P., Contoux, C., Cozic, A., & Cugnet, D. Implementation of the CMIP6 Forcing Data in the IPSL-CM6A-LR Model, *Journal of Advances in Modeling Earth Systems*, 12 (2020)

15. Hajima, T., et al. Development of the MIROC-ES2L Earth system model and the evaluation of biogeochemical processes and feedbacks, *Geoscientific Model Development*, 13 (2020).

16. Tatebe, H., et al. Description and basic evaluation of simulated mean state, internal variability, and climate sensitivity in MIROC6, *Geoscientific Model Development*, 12 (2019)

17. Müller, W., Jungclaus, J., Mauritsen, T., Baehr, J., Bittner, M., Budich, R., Bunzel, F., Esch, M., Ghosh, R., Haak, H., & Ilyina, T.: A Higher-resolution Version of the Max Planck Institute Earth System Model (MPI-ESM1. 2-HR), *Journal of Advances in Modeling Earth Systems*, 10 (2018)

18. Mauritsen, T., Bader, J., Becker, T., Behrens, J., Bittner, M., Brokopf, R., Brovkin, V., Claussen, M., Crueger, T., Esch, M., & Fast, I.. Developments in the MPI-M Earth System Model version 1.2 (MPI-ESM1. 2) and its response to increasing CO2, *Journal of Advances in Modeling Earth Systems*, 11 (2019)

19. Yukimoto, S., Kawai, H., Koshiro, T., Oshima, N., Yoshida, K., Urakawa, S., Tsujino, H., Deushi, M., Tanaka, T., Hosaka, M., & Yabu, S. The Meteorological Research Institute Earth System Model version 2.0, MRI-ESM2. 0: Description and basic evaluation of the physical component, *Journal of the Meteorological Society of Japan* (2019)

20. Cao, J.,Wang, B., Yang, Y.-M., Ma, L., Li, J., Sun, B., Bao, Y., He, J., Zhou, X., & Wu, L. The NUIST Earth System Model (NESM) version 3: description and preliminary evaluation, *Geoscientific Model Development*, 11 (2018)

21. Tjiputra, J. F., Schwinger, J., Bentsen, M., Morée, A. L., Gao, S., Bethke, I., Heinze, C., Goris, N., Gupta, A., He, Y.-C., Olivié, D., Seland, Ø., & Schulz, M. Ocean biogeochemistry in the Norwegian Earth System Model version 2 (NorESM2), *Geoscientific Model Development*, 13 (2020)

22. Park, S., Shin, J., Kim, S., Oh, E., & Kim, Y. Global climate simulated by the Seoul National university atmosphere model version 0 with a unified convection scheme (sam0-unicon), *Journal of Climate*, 32 (2019)

23. Sellar, A., Walton, J., Jones, C., Wood, R., Abraham, N., Andrejczuk, M., Andrews, M., Andrews, T., Archibald, A., de Mora, L., & Dyson, H. Implementation of UK Earth system models for CMIP6, *Journal of Advances in Modeling Earth Systems*, 12 (2020)

24. Heuzé, C., 2020. Antarctic Bottom Water and North Atlantic Deep Water in CMIP6 models. *Ocean Science Discussions* (2020)